

# We are IntechOpen, the world's leading publisher of Open Access books Built by scientists, for scientists

6,900

Open access books available

186,000

International authors and editors

200M

Downloads

Our authors are among the

154

Countries delivered to

TOP 1%

most cited scientists

12.2%

Contributors from top 500 universities



WEB OF SCIENCE™

Selection of our books indexed in the Book Citation Index  
in Web of Science™ Core Collection (BKCI)

Interested in publishing with us?  
Contact [book.department@intechopen.com](mailto:book.department@intechopen.com)

Numbers displayed above are based on latest data collected.  
For more information visit [www.intechopen.com](http://www.intechopen.com)



# New Energy Management Concepts for Hybrid and Electric Powertrains: Considering the Impact of Lithium Battery and Ultracapacitor Aging

*Francis Assadian, Kevin Mallon and Brian Walker*

## Abstract

During the lifetime of an energy storage system, its health deteriorates from use due to irreversible internal changes to the system. This degradation results in decreased capacity and efficiency of the battery or capacitor. This chapter reviews empirical aging models for lithium-ion battery and ultracapacitor energy storage systems. It will explore how operating conditions like large currents, high temperature, or deep discharge cycles impact the health of the energy storage system. After reviewing aging models, this chapter will then show how these models can be used in vehicle energy management control systems to reduce energy storage system aging. This includes both aging-aware control and control of hybrid energy storage systems (systems that include both a battery and an ultracapacitor).

**Keywords:** electric vehicle, hybrid vehicle, energy management, lithium ion, ultracapacitor, battery aging

## 1. Introduction

The internal combustion engine is a major contributor to greenhouse gas emissions and hydrocarbon pollution across the globe. Motor vehicles account for a major portion of pollutants such as carbon monoxide, nitrogen oxide, and volatile organic compounds [1]. Alternative powertrain vehicles (APVs), such as electric vehicles (EVs) and hybrid-electric vehicles (HEVs), are potential technological solutions to reduce transportation-sector emissions and fuel consumption. However, APVs require large amounts of battery-stored energy, which can be cost and weight prohibitive [2]. Degradation of the battery further adds to the lifetime cost of an APV, and battery degradation rate has been shown to be inversely correlated with fuel economy [3, 4]. Technologies that improve battery lifespan and fuel economy will reduce this lifetime cost and hasten the adoption of sustainable transportation.

Lithium-based batteries serve as the current main battery of choice for vehicle transportation because of their high energy density and ability for high cycle life. Improving cycle life of lithium batteries means limiting large currents in and out of

the battery as much as possible to lower degradation and heat affects.

Ultracapacitors (UC) can be added to vehicles to improve battery life by taking excess power away from the battery and storing it in temporary energy storage [5]. Capacitors can quickly unload power back into the system for high load situations such as a hard acceleration, taking away the need for a high-power drain from the battery.

This chapter will begin with a brief review of existing literature on empirical modeling of lithium-ion battery and ultracapacitor degradation. Then, a few select aging models will be reoriented for use in an APV energy management system (EMS). Finally, an example showing how to utilize these control-oriented models will be shown.

## 2. Energy storage aging review

### 2.1 Lithium ion battery aging

Aging of batteries is primarily caused by the formation of substrates in the chemical reaction pathways and the formation of cracks in the electrode materials from repeated stress cycles [6]. These aging mechanisms are accelerated by high charge and discharge rates, extreme battery temperatures, and deep depths of discharge [7]. Aging of the battery causes capacity fade (a decrease in the charge storage capacity) and power fade (a decrease in the battery efficiency). However, models of the cell chemistry that include the thermal and stress/strain relationships used to describe aging are computationally intensive and are ill-suited for use in APV EMSs [6, 8].

Research of battery aging in APVs instead tends to utilize empirical models [4, 9–14]. Using empirical aging models for vehicle battery degradation analysis provides a good trade-off between precision and complexity. These empirical models do not consider the physical or chemical processes of the battery degradation but instead approximate the battery's health by fitting experimental data to aging factors like charge throughput, calendar life, and number of charge/discharge cycles.

For instance, Refs. [9, 10, 15, 16] develop aging models that relate charge throughput to degradation, with temperature and current magnitude as additional stress factors. Refs. [17, 18] include depth of discharge as an additional stress factor, while [18] also distinguishes the impact of charging and discharging currents on battery degradation. The aging models for hybrid vehicle applications in [13, 14] consider a number of charge/discharge cycles and calendar life and use temperature, depth of discharge, and average state of charge as aging stress factors. Other models in the literature such as [8, 19, 20] use simple cycle counting to measure the state of health.

Current research works to integrate battery aging dynamics into these EMSs to form controllers that actively regulate battery degradation. In Ref. [4], the authors developed an SDP-based EMS for a parallel-HEV passenger vehicle that accounted for battery wear by mapping operating conditions to substrate growth, and associating substrate growth with battery state of health. The authors also analyzed how reducing battery aging increased the fuel consumption. In Refs. [4, 21], the authors developed a deterministic EMS for a parallel-HEV passenger vehicle that regulates battery degradation using a “severity factor” map: the control policy penalizes battery usage by an amount related to the severity of the operating conditions (in terms of temperature and current magnitude). The authors of [4] also showed an inverse correlation between the battery aging and fuel consumption.

## 2.2 Ultracapacitor aging

Lithium batteries have a high energy density but low power density, meaning that although they store large amounts of energy, that energy cannot be accessed quickly. Additionally, high currents to and from the battery are a stress factor for battery degradation. A potential solution to these problems is to integrate UCs into the energy storage system. UCs store energy in the electric field of an electrochemical double layer and have a high power density but low energy, allowing them to serve as complements to battery energy storage [5]. By integrating UCs into the powertrain, it becomes possible to meet the vehicle power requirements with a smaller battery and reduce battery degradation by restricting the magnitude of the current going to or from the battery [5, 22]. Aging of UCs is primarily dependent on time, temperature, and cell voltage [23–25].

Current research is interested in optimal control and sizing of the UC to reduce battery aging [26], and in particular how battery aging and fuel economy are jointly impacted. Some related work includes Ref. [27], in which the authors develop an optimal control policy to govern UC behavior and demonstrate clear aging improvements over a passive (uncontrolled) system. Refs. [28, 29] carried out a parametric study on battery degradation versus UC size in EVs, using a rule-based control system to govern power allocation. Ref. [30] developed a control strategy integrating UCs with lead-acid batteries in a HEV for battery life extension, and found that a 50% increase in battery cycle life would be needed for the UC to be cost-effective. Ref. [31] experimentally demonstrated a decrease in battery power fade and temperature rise in lithium-ion batteries due to UCs on an EV load profile.

## 3. Control-oriented aging

Meeting this goal of mitigating energy storage system degradation in APVs through control requires forming simplified models of the battery aging dynamics that can be included in or be used to generate an EMS. This chapter will summarize several approaches in the literature for using energy storage aging models for control applications.

### 3.1 Power-law model

Ref. [15] developed a lithium-ion battery empirical aging model for normalized battery capacity loss  $Q_{loss}$ , based on an Arrhenius equation. The model uses experimental data to relate battery degradation to on charge throughput  $Ah$  (in ampere-hours), current  $I_b$  (in C), and temperature  $T$  (in K).

$$Q_{loss} = A(I_b) \exp\left(\frac{-E_a + B|I_b|}{RT}\right) Ah^z \quad (1)$$

$E_a$ ,  $B$ , and  $z$  are fitted parameters, while  $A(I_b)$  is a fitted function of current.  $R$  is the ideal gas constant. Here,  $Q_{loss} = 0$  indicates a new battery, while  $Q_{loss} = 0.2$ , for example, indicates a 20% decrease in the storage capacity. This model treats current and temperature as static values. So, Eq. (1) can be differentiated to form a dynamic aging model as follows:

$$\frac{dQ_{loss}}{dt} = A(I_b) \exp\left(\frac{-E_a + B|I_b|}{RT}\right) \cdot z(Ah)^{z-1} \frac{dAh}{dt} \quad (2)$$

This model of aging has been used for aging control in, for example, [3, 4, 12].

### 3.2 Cycle life model

The Palmgren-Miner (PM) rule is a common method for analyzing fatigue life in mechanical systems and has been shown to effectively approximate the battery health over nonuniform charge and discharge cycles [8, 32, 33]. As per the PM rule, each charge and discharge cycle is considered to damage the battery by an amount related to the cycle life at that cycle's depth of discharge, charge and discharge current, and temperature. Ref. [18], for instance, models the cycle life of a battery as a function of depth of discharge  $DoD$ , charging current  $I_c$ , discharging current  $I_d$ , and temperature  $T$ .

$$CL = f(DoD, I_c, I_d, T) \quad (3)$$

Assume there is a charge-discharge cycle  $k$  with operating conditions  $DoD_k$ ,  $I_{c,k}$ ,  $I_{d,k}$ , and  $T_k$ , and so the cycle life for these operating conditions is  $CL_k$ . Then, under the PM rule, the damage  $D_k$  from cycle  $k$  is assumed to be

$$D_k = 1/CL_k \quad (4)$$

For multiple charge and discharge cycles, the damage from each cycle can be added to find the total damage  $D_{tot}$ . For the total damage up to cycle  $k$ ,

$$D_{tot}(k) = \sum_{i=1}^k D_i \quad (5)$$

Cumulative damage of zero denotes that the battery is unaged while cumulative damage of one means the battery has reached the end of its life. Typically, 20% capacity fade indicates a battery's end of life. So,

$$Q_{loss}(k) = 0.2 \cdot D_{tot}(k) \quad (6)$$

However, the above method does not readily lend itself to use in control; full charge and discharge cycles can take a long time to develop, and the EMS must act at a faster rate. One possibility is that the energy management system could consider how its decision would cause the damage of the current cycle to grow or lessen. For instance, consider a battery to be at operating conditions  $DoD_j$ ,  $I_{c,j}$ ,  $I_{d,j}$ , and  $T_j$ . The EMS then makes some decision such that the operating conditions become  $DoD_k$ ,  $I_{c,k}$ ,  $I_{d,k}$ , and  $T_k$ . Using Eqs. (3) and (4), the change in damage due to the EMS's decision can be calculated as

$$\Delta D = D_k - D_j = \frac{1}{f(DoD_k, I_{c,k}, I_{d,k}, T_k)} - \frac{1}{f(DoD_j, I_{c,j}, I_{d,j}, T_j)} \quad (7)$$

Then, Eq. (7) could be used in formulating an energy management strategy, such that the EMS would seek to minimize the additional damage caused by each decision it makes.

### 3.3 Ultracapacitor aging

Ref. [23] provides the following model for ultracapacitor aging, where  $SoA$  is the state of aging where 0 indicates start of life and 1 indicates end of life.

$$\frac{dSoA}{dt} = \frac{1}{T_{life}^{ref}} \cdot \exp\left(\ln(2) \frac{\theta_c - \theta_c^{ref}}{\theta_0}\right) \cdot \left(\exp\left(\ln(2) \frac{V - V^{ref}}{V_0}\right) + K\right) \quad (8)$$

where  $\theta_c$  is the UC temperature,  $V$  is the UC voltage, and the remaining variables ( $T_{life}^{ref}$ ,  $\theta_c^{ref}$ ,  $\theta_0$ ,  $V^{ref}$ ,  $V_0$ , and  $K$ ) are experimentally fitted parameters. This model is ready to be used for control as is. Ref. [23] defines the UC end-of-life condition as similar to batteries: when the capacitance of the UC has faded by 20%.

#### 4. Case study: electric vehicle with hybrid energy storage

This section develops a model for a hybrid energy storage system electric vehicle (HESS-EV)—specifically, an electric bus that uses a lithium-ion battery pack for energy storage and an ultracapacitor pack for handling large power requests. This example study will be used to show how active control of aging factors can improve the lifespan of the energy storage system without compromising energy consumption. This system is depicted in **Figures 1** and **2**.

##### 4.1 Vehicle dynamics

For this study, a backward-facing quasi-static vehicle model [34] is used to represent the vehicle dynamics. In this model, it is assumed that the driver accurately follows the velocity of a given drive cycle, eliminating the need for a driver model and allowing the time-history of the electrical load placed on the powertrain to be calculated in advance.

This vehicle model, illustrated in **Figure 3**, considers inertial forces, aerodynamic drag, and rolling resistance (note that road incline is neglected for this chapter). The drag force is given by

$$F_{drag} = \frac{1}{2} \rho A_f C_D v_v^2 \quad (9)$$

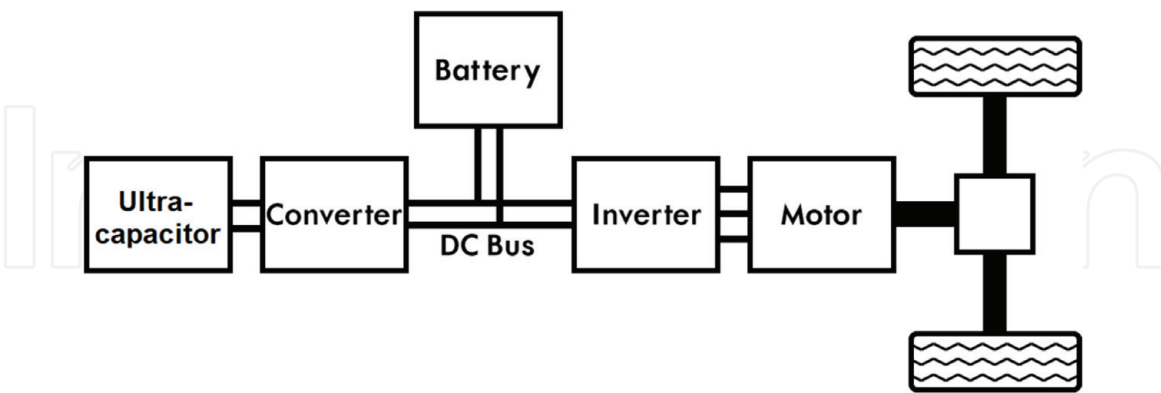


**Figure 1.**  
HESS-EV model.

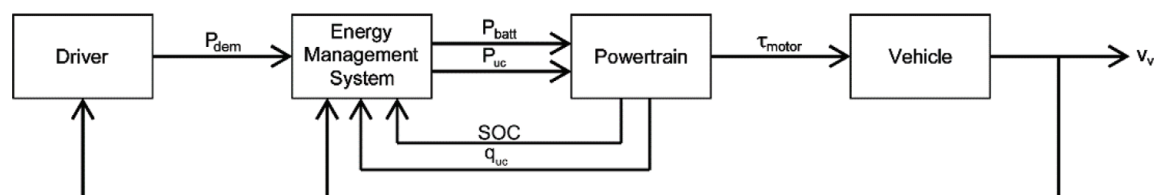


**Figure 2.**  
HESS-EV block diagram.

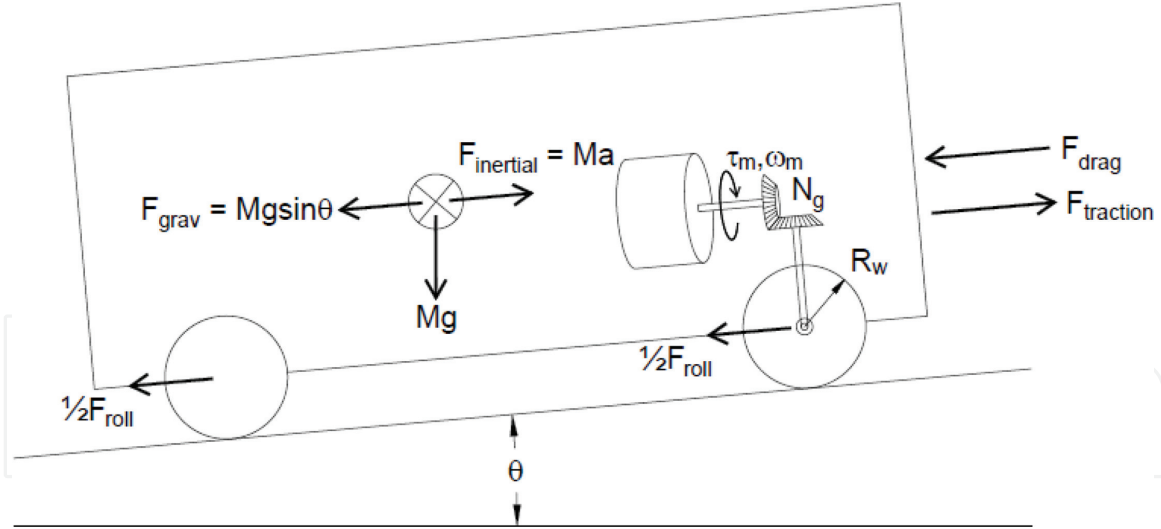


**Figure 3.**  
Vehicle diagram.

where  $\rho$  is the air density,  $A_f$  is the frontal area,  $C_D$  is the drag coefficient, and  $v_v$  is the vehicle velocity. Rolling resistance is given by

$$F_{roll} = M_v g C_R \quad (10)$$

where  $M_v$  is the vehicle's total mass,  $g$  is the acceleration due to gravity, and  $C_R$  is the rolling resistance coefficient. In a backward-facing model, the inertial force is determined from the vehicle acceleration and the vehicle mass as

$$F_{inertial} = M_{eq} \frac{dv_v}{dt}. \quad (11)$$

$M_{eq}$  is the mass of the bus plus the equivalent mass due to the rotational inertia of the motor and wheels.

$$M_{eq} = M_v + 4J_w \left( \frac{1}{R_w} \right)^2 + J_m \left( \frac{N_{fd} N_{gb}}{R_w} \right)^2, \quad (12)$$

where  $J_w$  is the rotational inertia of one wheel,  $J_m$  is the rotational inertia of the motor,  $R_w$  is the wheel radius,  $N_{fd}$  is the final drive ratio, and  $N_{gb}$  is the gearbox ratio. The acceleration term in Eq. (11) is approximated from a given velocity profile according to

$$\frac{dv_v}{dt}(t) \approx \frac{v_v(t + \Delta t) - v_v(t - \Delta t)}{2\Delta t}. \quad (13)$$

The inertial, drag, and rolling resistance forces sum together to give the traction force on the bus.

$$F_{traction} = F_{inertial} + F_{drag} + F_{roll} \quad (14)$$

Parameter values for the vehicle model can be found in **Table 1**. The bus is assumed to be fully loaded and at its maximum allowable weight. Vehicle parameters are estimated from existing literature on bus simulation [35–37].

Parameter	Variable	Value
Vehicle mass	$M_v$	18,181 kg
Frontal area	$A_f$	8.02 m <sup>2</sup>
Drag coefficient	$C_D$	0.55
Roll resistance coefficient	$C_R$	0.008
Wheel inertia	$J_w$	20.52 kg-m <sup>2</sup>
Motor inertia	$J_m$	0.277 kg-m <sup>2</sup>
Wheel radius	$R_w$	0.48 m
Final drive ratio	$N_{fd}$	5.1:1
Gearbox ratio	$N_{gb}$	5:1

**Table 1.**  
 Vehicle physical parameters.

## 4.2 Powertrain model

This subsection describes the modeling of the HESS-EV powertrain, including the transmission, motor, battery, and ultracapacitor subsystems, as indicated in **Figure 1**. The goal of the vehicle model is to capture the primary forces on the vehicle while maintaining model simplicity. Both these make simulation of the system easier and make optimal control methods, such as dynamic programming or model-predictive control, less computationally complex. Otherwise, the energy management system might suffer from the “curse of dimensionality”.

### 4.2.1 Transmission

Next, the vehicle speed and traction force are transformed into motor torque and motor speed. Assuming transmission efficiency of  $\eta_{trans}$ , represented as torque losses, the motor torque is given by

$$\tau_m = \begin{cases} \left( \frac{R_w}{N_{fd}N_{gb}} F_{traction} \right) / \eta_{trans} & F_{traction} \geq 0 \\ \left( \frac{R_w}{N_{fd}N_{gb}} F_{traction} \right) \cdot \eta_{trans} & F_{traction} < 0 \end{cases} \quad (15)$$

and the motor speed is given by

$$\omega_m = \frac{N_{fd}N_{gb}}{R_w} v_v \quad (16)$$

Then, the mechanical power needed to drive the vehicle  $P_{mech}$  can be expressed in terms of the motor torque and angular velocity.

$$P_{mech} = \tau_m \cdot \omega_m \quad (17)$$

Here, positive  $P_{mech}$  indicates acceleration. Parameter values for the transmission can be found in **Table 1**.

#### 4.2.2 Motor and power electronics

The electrical power demand of the motor,  $P_{dem}$ , is calculated from  $P_{mech}$  and an efficiency parameter  $\eta_{motor}$ ,  $0 < \eta_{motor} < 1$ .  $\eta_{motor}$  is a function of  $\tau_m$  and  $\omega_m$  and is determined from a static efficiency map.

$$P_{dem} = \begin{cases} P_{mech}/\eta_{trans} & \tau_m \geq 0 \\ P_{mech} \cdot \eta_{trans} & \tau_m < 0 \end{cases} \quad (18)$$

The efficiency map is obtained from the National Renewable Energy Laboratory's Advanced Vehicle Simulator (ADVISOR) data library [38] and scaled to the appropriate size using the scaling method in [5]. It includes both the motor efficiency and the efficiency of the power electronics. The modeled vehicle utilizes a 250 kW AC induction motor.

The power demand for the electric motor is provided by battery power  $P_{batt}$  and ultracapacitor power  $P_{uc}$ . As part of the quasi-static simulation, it is assumed that the power demand is always met.

$$P_{dem} = P_{batt} + P_{uc} \quad (19)$$

Because  $P_{dem}$  is set by the drive cycle and  $P_{uc}$  is a controlled variable,  $P_{batt}$  is fixed and dependent on both  $P_{dem}$  and  $P_{uc}$ . Therefore, Eq. (19) can be rewritten as

$$P_{batt} = P_{dem} - P_{uc} \quad (20)$$

### 4.3 Energy storage systems

The previous subsections detailed how the driver's electrical power request would be determined. As depicted in **Figure 4**, the EMS decides how that power is split between the lithium-ion battery and the ultracapacitor. This subsection will first detail the modeling of the battery, followed by modeling of the ultracapacitor.

#### 4.3.1 Battery

This HESS-EV uses lithium-ion batteries represented by the simple battery model shown in **Figure 5**, where  $V_{cell}$  is the open-circuit voltage (OCV) of a single battery cell, while  $R_{cell}$  represents the combined effects of ohmic resistances, diffusion resistances, and charge-transfer resistances [5]. This quasistatic model requires only a single state variable, state of charge (SOC). The OCV as well as the resistance are considered to vary with SOC per experimental data for a lithium-iron-phosphate battery [39].

The equivalent resistance of the complete battery pack is given by

$$R_{eq} = R_{cell} \frac{N_{ser}}{N_{par}} \quad (21)$$

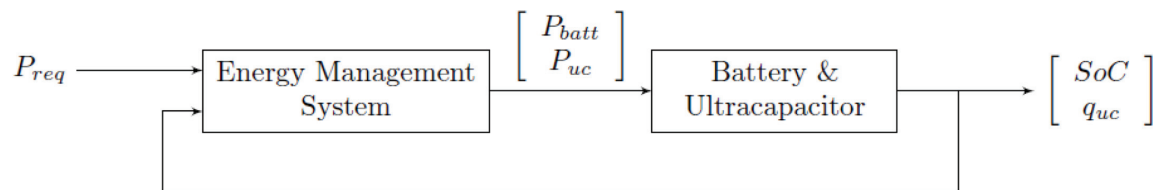


**Figure 4.**  
Battery and UC block diagram.

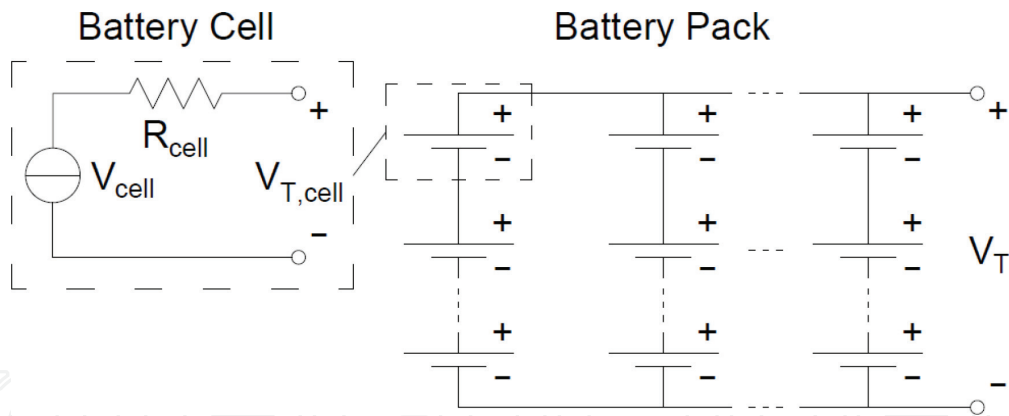


**Figure 5.**  
 Battery cell and battery pack equivalent circuit.

where  $N_{ser}$  is the number of cells in series,  $N_{par}$  is the number in parallel, and  $R_{cell}$  is the resistance of a single cell. The open circuit voltage of the vehicle battery pack is likewise given by

$$V_{ocv} = N_{ser} \cdot V_{cell} \quad (22)$$

Using the equivalent circuit in **Figure 4**, the battery terminal voltage can be found from the OCV and battery power  $P_{batt}$  as follows:

$$I_{batt} = P_{batt} / V_T \quad (23)$$

$$V_T = V_{ocv} - I_{batt} \cdot R_{eq} \quad (24)$$

Then, substituting Eq. (23) into Eq. (24) and solving yields

$$V_T^2 = V_{ocv} \cdot V_T - P_{batt} R_{eq} \quad (25)$$

$$V_T = \frac{1}{2} \left( V_{ocv} + \sqrt{V_{ocv}^2 - 4P_{batt}R_{eq}} \right) \quad (26)$$

$V_T$  can then be substituted back into Eq. (23) to obtain the battery current, which can be integrated to obtain the state of charge.

$$SOC(k+1) = SOC(k) + \Delta t \cdot \frac{I_{batt}}{Q_{batt}}, \quad (27)$$

where  $Q_{batt}$  is the capacity of the battery pack in coulombs and  $\Delta t$  is the timestep.

The parameters for the battery model can be found in **Table 2**. The number of cells in series was chosen so that the OCV would be in line with the

Parameter	Variable	Value
Battery cells in parallel	$N_{par}$	400 cells
Parallel sets in series	$N_{ser}$	100 sets
Total charge capacity	$Q_{batt}$	340 Ah
Battery temperature	$T$	35°C.

**Table 2.**  
 Battery parameters.

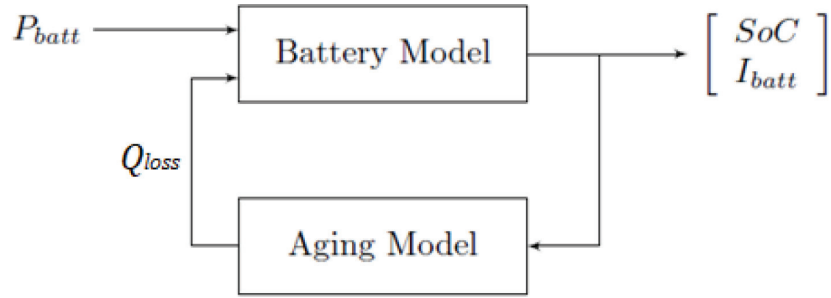


**Figure 6.**  
Battery aging and dynamics block diagram.

recommendations in [40]. The number of cells in parallel was chosen so that the bus can be driven for 4 hours continuously to meet the power requirements of [40, 41].

For this example, the cycle counting method described in Eqs. (3)–(7) is used, with the aging model in Ref. [18] used to determine cycle life. This is illustrated in **Figure 6**. The battery is assumed to operate at a constant 35°C.

#### 4.3.2 Ultracapacitor

The ultracapacitor model is similar in nature to the battery model, so the dynamics here will be presented more briefly. For this study, a second-order equivalent circuit based on the 100F ultracapacitor model in [42] is used to model the individual ultracapacitors. Parameters for this model are given in **Table 3**. Like with the battery, the ultracapacitor pack consists of ultracapacitors arranged in series and parallel as shown in **Figure 7**.

As shown in **Figure 1**, the UC is connected to the DC bus through a converter, so that the voltage of the UC pack is independent of the voltage at the DC bus. The ultracapacitor pack takes on total power  $P_{uc}$  and has  $N_{pc}$  cells in parallel per set and  $N_{sc}$  sets of cells in series. Then, the power going to each individual cell is

$$P_{uc,cell} = \frac{P_{uc}}{N_{pc}N_{sc}} \quad (28)$$

Let  $q_1$  be the charge that corresponds to the  $C_1$  capacitor, and let  $q_2$  be the charge that corresponds to the  $C_2$  capacitor. For a given power  $P_{uc,cell}$ , the current and terminal voltage can be found in a similar manner to Eqs. (23)–(26).

$$I_{uc} = P_{uc,cell}/V_{T,uc} \quad (29)$$

$$V_{T,uc} = q_2/C_2 - I_{uc}R_2 \quad (30)$$

Parameter	Variable	Value
UC parallel cells	$N_{pc}$	100
UC series sets	$N_{sc}$	100
Resistor 1	$R_1$	29.6 mΩ
Capacitor 1	$C_1$	31.7 F
Resistor 2	$R_2$	14.7 mΩ
Capacitor 2	$C_2$	74.1781 F
Temperature	$\theta$	45°C

**Table 3.**  
Ultracapacitor parameters.

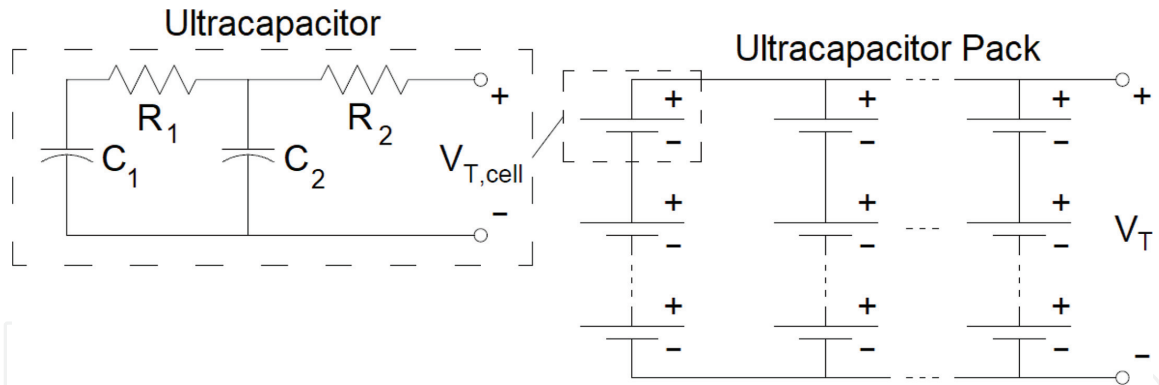


**Figure 7.**  
 Ultracapacitor pack equivalent circuit.

Then, substituting Eq. (23) into Eq. (24) and solving yields

$$V_{T,uc}^2 = q_2/C_2 \cdot V_{T,uc} - P_{batt}R_{eq} \quad (31)$$

$$V_{T,uc} = \frac{1}{2} \left( q_2/C_2 + \sqrt{q_2^2/C_2^2 - 4P_{uc,cell}R_2} \right) \quad (32)$$

$V_T$  can then be substituted back into Eq. (23) to obtain the battery current. Then, the state equations for the two capacitors are

$$\dot{q}_1 = 1/R_1 (q_1/C_1 - q_2/C_2) \quad (33)$$

$$\dot{q}_2 = I_{uc} - 1/R_1 (q_1/C_1 - q_2/C_2) \quad (34)$$

The total charge in the capacitor  $q_{uc}$  is given by

$$q_{uc} = q_1 + q_2 \quad (35)$$

For this example, the cycle counting model in [23] and Section 3.3 is used. This is illustrated in **Figure 8**. The ultracapacitor is assumed to operate at a constant 45°C.

#### 4.4 Energy management system

A deterministic dynamic programming (DDP) controller is used for the EMS. DDP is a form of optimal control—in this example, the DDP controller solves the following optimization problem over a known velocity profile that is  $N$  steps long. For this system, the minimum, target, and maximum charge are  $q_{min} = 50$  C,  $q_{tgt} = 150$  C, and  $q_{max} = 250$  C, and the minimum and maximum UC power are  $P_{uc,min} = -62.5$  W and  $P_{uc,max} = 62.5$  W so as not to exceed manufacturer specified operating conditions [42]. Note that these are constraints on each cell, not the entire pack. The battery power constraints will be discussed shortly.

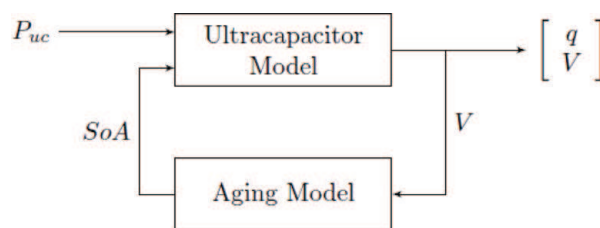


**Figure 8.**  
 Ultracapacitor aging & dynamics block diagram.

$$\begin{aligned}
& \text{minimize } \sum_{i=0}^N \left( q_{uc}(i) - q_{uc,tgt} \right)^2 + Q_1 \cdot (\Delta D(i))^2 \\
& \text{subject to } q_{min} < q_{uc} < q_{max} \\
& P_{uc,min} < P_{uc} < P_{uc,max} \\
& P_{batt,min} < P_{batt} < P_{batt,max}
\end{aligned} \tag{36}$$

In plain terms, the DDP controller finds how to split power between the battery and ultracapacitor in such a way as to

1. Keep the UC charge near a target value
2. Minimize the aging of the battery
3. Ensure that the UC charge, UC power, and battery power stays within given bounds

The method to solve DDP problems can be found in Ref. [5].

In order to demonstrate the benefit of actively controlling aging, two versions of the controller will be tested:

1. Load-leveling DDP:  $Q_1$  is set to zero. A battery power constraint of  $P_{batt,min} = -3.2W$  and  $P_{batt,max} = 3.2W$  per cell prevents large power (and therefore large current) going to the battery, and the cost function will bring the UC charge back to the target afterwards.
2. Active Aging Control: Battery power is unconstrained, but battery damage is directly penalized. A range of values are used for  $Q_1$ .

#### 4.5 Simulation

The HESS-EV is simulated on the Manhattan Bus Cycle [43]—an urban bus velocity profile—for 4 hours at a time. After each simulation, the aging for the battery and ultracapacitor is measured. The battery capacity and ultracapacitor capacitances are then updated, and the next simulation begins. This process is repeated until the battery reaches its end of life.

#### 4.6 Results

The lifespan of the battery in years is estimated by measuring the total kilometers driven before the battery reached the end of its life, and then using the Federal Highway Administration's average annual kilometers driven by transit busses [44] to convert the kilometers driven into an approximate number of years. Additionally, the ultracapacitor degradation and average kWh/km for the HESS-EV over the lifespan of the battery are measured.

**Figure 9** shows a comparison between battery lifespan and fuel economy for both controller types. Clearly, the aging-aware control outperforms the load-leveling type controller: In all cases, the battery with actively-controlled aging has a longer lifespan.

Additionally, this figure shows a trade-off between efficiency and battery lifespan: As the battery lifespan increases with greater penalties on battery damage, the energy efficiency of the vehicle drops. This is because greater penalties on aging cause more current to pass through UC in order to reduce the load on the battery. In

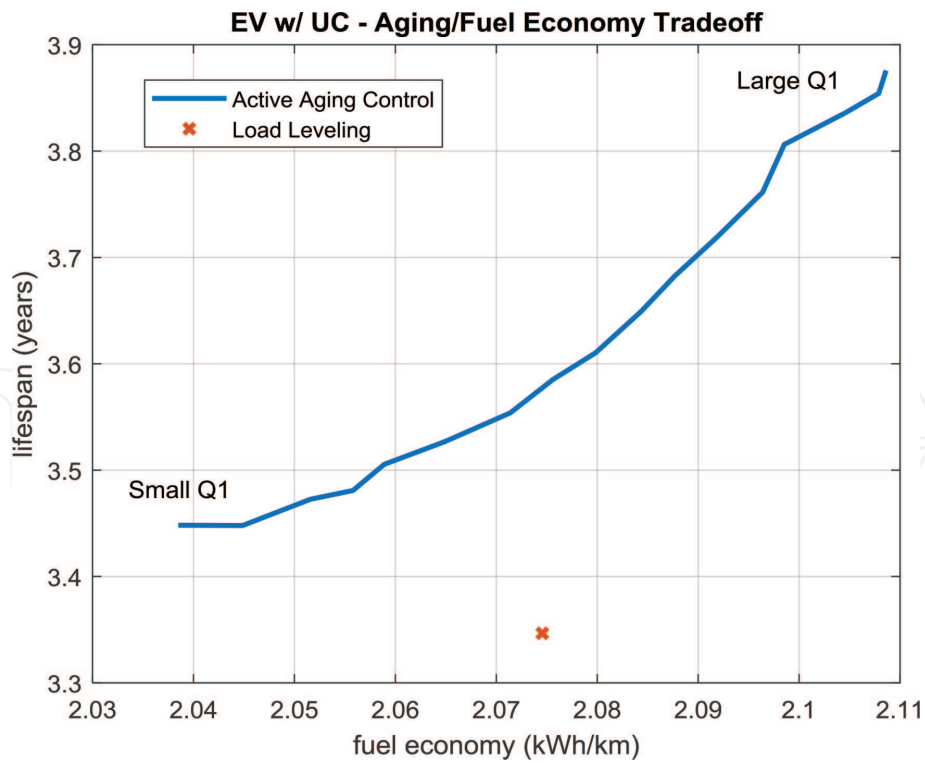


**Figure 9.**  
 Lifespan vs. fuel economy for HESS-EV, where  $Q_1$  is the penalty on battery damage.

turn, there are more power losses due to the internal resistances of the capacitor pack. This is illustrated in **Figure 10**, which shows the charge in the UC for two different values of  $Q_1$ . One can see how a small penalty on  $Q_1$  means the controller will focus mostly on keeping the UC charge near the target value; this in turn means less current through the UC, so less power losses from the UCs.

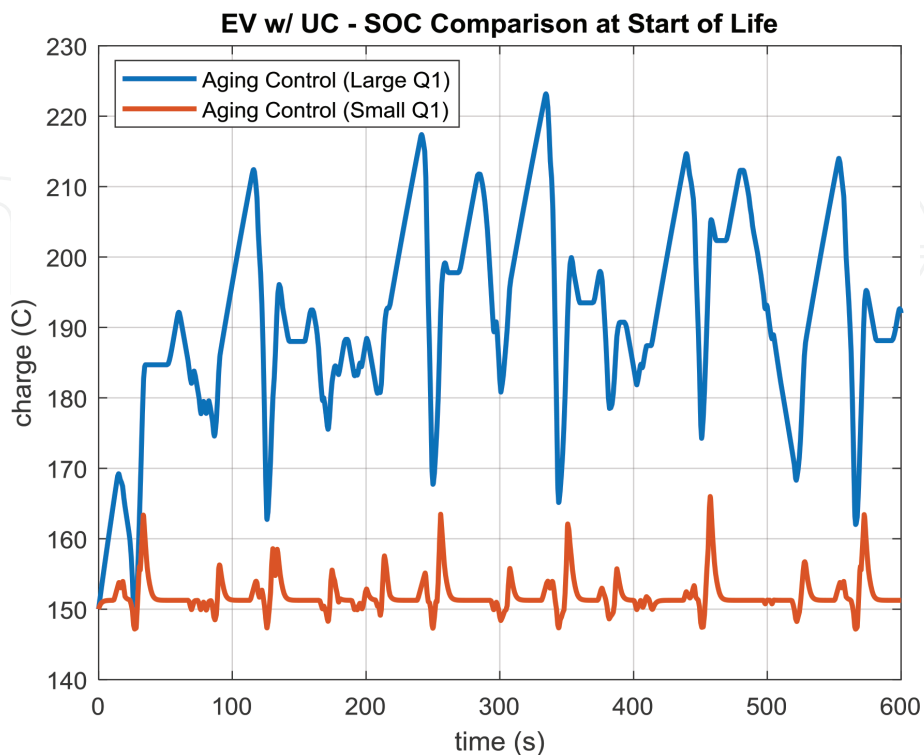


**Figure 10.**  
 Ultracapacitor charge for two different values of  $Q_1$ .

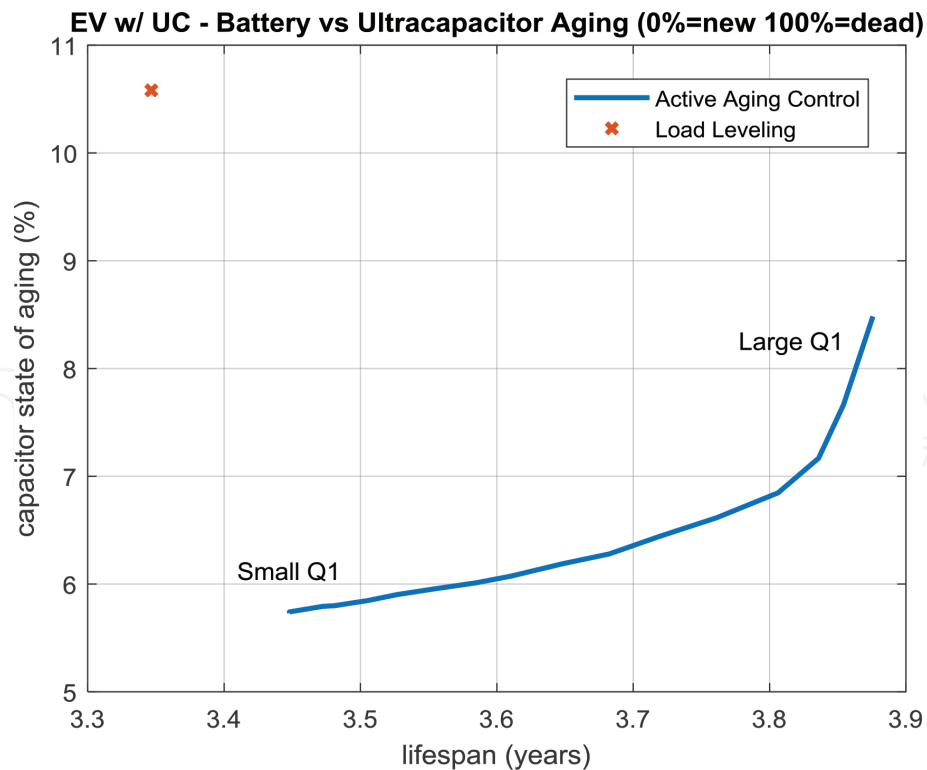


**Figure 11.** Battery lifespan vs. UC aging.  $Q_1$  is the penalty on battery damage.

**Figure 11** shows the relationship between battery degradation and ultracapacitor degradation. Two things are apparent: one, there is an inverse relationship between the two—increasing battery lifespan comes at the cost of reducing ultracapacitor lifespan. A cause of this can be observed in **Figure 10**. Second, ultracapacitor degradation happens much more slowly than battery degradation. Despite the battery reaching the end of its lifespan, the ultracapacitor ages no more than 6–11%.

## 5. Conclusions

Deterioration of energy storage systems is inevitable, but by understanding the process it becomes possible to control and slow the capacity and efficiency fade. This chapter covered empirical aging models for lithium-ion and ultracapacitor systems and their use in vehicle energy management. First, existing work on different lithium ion and ultracapacitor aging models was reviewed, as well as those models' application in energy management control strategies. After reviewing aging models and discussing how to adapt empirical aging models for control, a case study was carried out on an ultracapacitor-augmented electric vehicle to show how actively controlling aging can improve an EMS. This case study included the steps necessary to model the vehicle and powertrain dynamics as well as simple or quasistatic models of the battery and ultracapacitor. DDP was generally used in two types of controllers: a load-leveling type controller that was unaware of aging dynamics, and a “smart” controller that incorporated battery aging dynamics into its design. When simulated, the aging-aware controller outperformed the simple controller, offering longer battery lifespan without any cost in fuel economy or vehicle performance. This demonstrates how advanced control—making EMSs aware of energy storage aging dynamics—can improve the efficiency and viability of alternative powertrain vehicles.

## **Acknowledgements**

This work was supported by the University of California, Davis and by the Vertically Integrated Projects (VIP) program at UC Davis.

## **Conflict of interest**

The authors declare no conflict of interest.

IntechOpen

IntechOpen

## **Author details**

Francis Assadian\*, Kevin Mallon and Brian Walker  
University of California—Davis, Davis, CA, USA

\*Address all correspondence to: [fassadian@ucdavis.edu](mailto:fassadian@ucdavis.edu)

## **IntechOpen**

---

© 2019 The Author(s). Licensee IntechOpen. This chapter is distributed under the terms of the Creative Commons Attribution License (<http://creativecommons.org/licenses/by/3.0>), which permits unrestricted use, distribution, and reproduction in any medium, provided the original work is properly cited. 

## References

- [1] Abdel-Rahman A. On the emissions from internal-combustion engines: A review. *International Journal of Energy Research*. 1998;**22**:483-513
- [2] Lee T-K, Filipi Z. Impact of model-based lithium-ion battery control strategy on battery sizing and fuel economy in heavy-Duty HEVs. *SAE International Journal of Commercial Vehicles*. 2011;**4**:198-209
- [3] Moura SJ, Stein JL, Fathy HK. Battery-health conscious power management in plug-in hybrid electric vehicles via electrochemical modeling and stochastic control. *IEEE Transactions on Control Systems Technology*. 2013;**21**:679-694
- [4] Suri G, Onori S. A control-oriented cycle-life model for hybrid electric vehicle lithium-ion batteries. *Energy*. 2016;**96**:644-653
- [5] Guzzella L, Sciarretta A. *Vehicle Propulsion Systems*. 3rd ed. Berlin, Heidelberg: Springer Berlin Heidelberg; 2013. DOI: 10.1007/978-3-642-35913-2
- [6] Ramadesigan V, Northrop PWC, De S, Santhanagopalan S, Braatz RD, Subramanian VR. Modeling and simulation of lithium-ion batteries from a systems engineering perspective. *Journal of the Electrochemical Society*. 2012;**159**:R31-R45
- [7] Pelletier S, Jabali O, Laporte G, Veneroni M. Battery degradation and behaviour for electric vehicles: Review and numerical analyses of several models. *Transportation Research Part B: Methodological*. 2017;**103**:163-164
- [8] Safari M, Morcrette M, Teyssot A, Delacourt C. Life-prediction methods for lithium-ion batteries derived from a fatigue approach I. Introduction: Capacity-loss prediction based on damage accumulation. *Journal of the Electrochemical Society*. 2010;**157**:A713-A720
- [9] Petit M, Prada E, Sauvant-Moynot V. Development of an empirical aging model for Li-ion batteries and application to assess the impact of vehicle-to-grid strategies on battery lifetime. *Applied Energy*. 2016;**172**:398-407
- [10] Bishop JDK, Axon CJ, Bonilla D, Tran M, Banister D, McCulloch MD. Evaluating the impact of V2g services on the degradation of batteries in PHEV and EV. *Applied Energy*. 2013;**111**:206-218
- [11] Cordoba-Arenas A, Onori S, Rizzoni G. A control-oriented lithium-ion battery pack model for plug-in hybrid electric vehicle cycle-life studies and system design with consideration of health management. *Journal of Power Sources*. 2015;**279**:791-808
- [12] Onori S, Spagnol P, Marano V, Guezennec Y, Rizzoni G. A new life estimation method for lithium-ion batteries in plug-in hybrid electric vehicles applications. *International Journal of Power Electronics*. 2012;**4**:302-319
- [13] Millner A. Modeling lithium ion battery degradation in electric vehicles. In: *2010 IEEE Conference on Innovative Technologies for an Efficient and Reliable Electricity Supply*; IEEE. 2010. pp. 349-356
- [14] Guenther SB, Hennings W, Waldowski P, Danzer MA. Model-based investigation of electric vehicle battery aging by means of vehicle-to-grid scenario simulations. *Journal of Power Sources*. 2013;**239**:604-610
- [15] Wang J, Liu P, Hicks-Garner J, Sherman E, Soukiazian S, Verbrugge M, et al. Cycle-life model for

graphite-LiFePO<sub>4</sub> cells. *Journal of Power Sources*. 2011;**196**:3942-3948

[16] Spotnitz R. Simulation of capacity fade in lithium-ion batteries. *Journal of Power Sources*. 2003;**113**:72-80

[17] Sarasketa-Zabala E, Martinez-Laserna E, Berecibar M, Gandiaga I, Rodriguez-Martinez LM, Villarreal I. Realistic lifetime prediction approach for Li-ion batteries. *Applied Energy*. 2016;**162**:839-852

[18] Omar N, Monem MA, Firouz Y, Salminen J, Smekens J, Hegazy O, et al. Lithium iron phosphate based battery—Assessment of the aging parameters and development of cycle life model. *Applied Energy*. 2014;**113**:1575-1585

[19] DiOrio N, Dobos A, Janzou S, Nelson A, Lundstrom B. Technoeconomic Modeling of Battery Energy Storage in SAM. tech. rep., National Renewable Energy Laboratory (NREL) NREL/TP-6A20-64641; 2015

[20] Marano V, Onori S, Guezennec Y, Rizzoni G, Madella N. Lithium-ion batteries life estimation for plug-in hybrid electric vehicles. In: 2009 IEEE Vehicle Power and Propulsion Conference; Sept. 2009. pp. 536-543

[21] Cordoba-Arenas A, Onori S, Guezennec Y, Rizzoni G. Capacity and power fade cycle-life model for plug-in hybrid electric vehicle lithium-ion battery cells containing blended spinel and layered-oxide positive electrodes. *Journal of Power Sources*. 2015;**278**: 473-483

[22] Williamson SS. *Energy Management Strategies for Electric and Plug-in Hybrid Electric Vehicles*. New York, NY: Springer New York; 2013. DOI: 10.1007/978-1-4614-7711-2

[23] Kovaltchouk T, Multon B, Ahmed HB, Aubry J, Venet P. Enhanced aging model for supercapacitors taking into

account power cycling: Application to the sizing of an energy storage system in a direct wave energy converter. *IEEE Transactions on Industry Applications*. 2015;**51**:2405-2414

[24] Kovaltchouk T, Ahmed HB, Multon B, Aubry J, Venet P. An aging-aware life cycle cost comparison between supercapacitors and Li-ion batteries to smooth Direct Wave Energy Converter production. In: 2015 IEEE Eindhoven PowerTech; June 2015. pp. 1-6

[25] Hammar A, Venet P, Lallemand R, Coquery G, Rojat G. Study of accelerated aging of supercapacitors for transport applications. *IEEE Transactions on Industrial Electronics*. 2010;**57**:3972-3979

[26] Miller JM, Sartorelli G. Battery and ultracapacitor combinations #x2014; Where should the converter go? In: 2010 IEEE Vehicle Power and Propulsion Conference; 2010. pp. 1-7

[27] Song Z, Li J, Han X, Xu L, Lu L, Ouyang M, et al. Multi-objective optimization of a semi-active battery/supercapacitor energy storage system for electric vehicles. *Applied Energy*. 2014;**135**:212-224

[28] Shen J, Dusmez S, Khaligh A. Optimization of sizing and battery cycle life in battery/ultracapacitor hybrid energy storage systems for electric vehicle applications. *IEEE Transactions on Industrial Informatics*. 2014;**10**: 2112-2121

[29] Akar A, Tavlasoglu Y, Vural B. An energy management strategy for a concept battery/ultracapacitor electric vehicle with improved battery life. *IEEE Transactions on Transportation Electrification*. 2017;**3**:191-200

[30] Carter R, Cruden A, Hall PJ. Optimizing for efficiency or battery life in a battery/supercapacitor electric

- vehicle. *IEEE Transactions on Vehicular Technology*. 2012;**61**:1526-1533
- [31] Zhao C, Yin H, Ma C. Quantitative evaluation of LiFePO battery cycle life improvement using ultracapacitors. *IEEE Transactions on Power Electronics*. 2016;**31**:3989-3993
- [32] Zhou C, Qian K, Allan M, Zhou W. Modeling of the cost of EV battery wear due to V2G Application 621 in power systems. *IEEE Transactions on Energy Conversion*. 2011;**26**:1041-1050
- [33] Mallon KR, Assadian F, Fu B. Analysis of on-board photovoltaics for a battery electric bus and their impact on battery lifespan. *Energies*. 2017;**10**:943
- [34] Mohan G, Assadian F, Longo S. Comparative analysis of forward-facing models vs backwardfacing models in powertrain component sizing. In: *IET Hybrid and Electric Vehicles Conference 2013 (HEVC 2013)*; 2013. pp. 1-6
- [35] Zeng X, Yang N, Wang J, Song D, Zhang N, Shang M, et al. Predictive-model-based dynamic coordination control strategy for power-split hybrid electric bus. *Mechanical Systems and Signal Processing*. Aug. 2015;**60**:61:785-798
- [36] Sangtarash F, Esfahanian V, Nehzati H, Haddadi S, Bavanpour MA, Haghpanah B. Effect of different regenerative braking strategies on braking performance and fuel economy in a hybrid electric bus employing CRUISE vehicle simulation. *SAE International Journal of Fuels and Lubricants*. 2008;**1**(1):828-837
- [37] Wang BH, Luo YG, Zhang JW. Simulation of city bus performance based on actual urban driving cycle in China. *International Journal of Automotive Technology*. 2008;**9**(4): 501-507
- [38] Markel T, Brooker A, Hendricks T, Johnson V, Kelly K, Kramer B, et al. ADVISOR: A systems analysis tool for advanced vehicle modeling. *Journal of Power Sources*. 2002;**110**(2):255-266
- [39] Erdinc O, Vural B, Uzunoglu M. A dynamic lithium-ion battery model considering the effects of temperature and capacity fading. In: *2009 International Conference on Clean Electrical Power, ICCEP*; 2009. pp. 383-386. DOI: 10.1109/ICCEP.2009.5212025
- [40] Nelson RF. Power requirements for batteries in hybrid electric vehicles. *Journal of Power Sources*. 2000;**91**(1): 2-26
- [41] Fauvel C, Napal V, Rousseau A. Medium and heavy duty hybrid electric vehicle sizing to maximize fuel consumption displacement on real world drive cycles. Los Angeles, California: Power (W); 2012. pp. 0-22. Available from: <https://www.autonomie.net/docs/5%20-%20Presentations/Heavy%20duty/CF%20-%20EVS26.pdf>
- [42] Dougal RA, Gao L, Liu S. Ultracapacitor model with automatic order selection and capacity scaling for dynamic system simulation. *Journal of Power Sources*. 2004;**126**:250-257
- [43] Barlow TJ, Latham S, Mccrae IS, Boulter PG. A Reference Book of Driving Cycles for Use in the Measurement of Road Vehicle Emissions. TRL Published Project Report; 2009. Available from: <https://trid.trb.org/view/909274>
- [44] FHWA (Federal Highway Administration). *Highway Statistics 2013*; 2013